Modulation of HOXA9 after skeletal muscle denervation and reinnervation

Xiaomei Lu
Shanxi Medical University Second Affiliated Hospital https://orcid.org/0000-0002-5889-3337
Bingsheng Liang
Shanxi Medical University Second Affiliated Hospital
Shuaijie Li
Tongji University School of Medicine
Zhi Chen
Shanxi Medical University Second Affiliated Hospital
Wenkai Chang (cwk2020@sina.com)
https://orcid.org/0000-0002-8389-3136

Research

Keywords:

Posted Date: January 30th, 2020

DOI: https://doi.org/10.21203/rs.2.22314/v1

Abstract

Background HOXA9 (Homeobox A9), whose expression is promoted by MLL1 (Mixed Lineage Leukemia 1) and WDR5 (WD-40 repeat protein 5), is a homeodomain-containing transcription factor which plays an essential role in regulating stem cell activity. HOXA9 inhibits regeneration of skeletal muscle and delays the recovery after muscle wound in aged mice, but is little known in denervated/reinnervated muscles. Methods we performed detailed time-process expression analysis on HOXA9 and its promotors, MLL1 and WDR5, in the rat gastrocnemius muscle after three types of sciatic nerve surgeries: nerve transection (denervation); end-to-end repairing (repairing); and the sham operation. Then the specific mechanisms of Hoxa9 were detected in vitro through primary satellite cells transfected respectively by pIRES2-DsRed2 empty plasmids, pIRES2-DsRed2-HOXA9 plasmids, pPLK/ GFP -Puro empty plasmids, and pPLK/GFP-Puro- HOXA9 shRNA plasmids. Results We found that HOXA9 expression was synchronous with the severity of muscle atrophy, as well as the upregulation of MLL1 and WDR5 associated with the denervation state to some extent. Indeed, experiments with primary satellite cells revealed that HOXA9 inhibited myogenic differentiation, but not destroy the differentiation potential, influenced the best-known atrophic pathways, and promoted apoptosis. Conclusion HOXA9 may play a pro-atrophic role in denervated muscle atrophy.

Background

Skeletal muscle innervation plays a vital role in determining muscle structure and function [1]. Denervation not only leads to muscle atrophy with complex cascade reactions but also leads to poor prognosis and even increased mortality [2, 3].

Resulting from the imbalance between the synthesis and degradation of myoprotein, myofibers atrophy of myofibers progressed rapidly in diameter, mass, weight, and strength after denervation [4, 5]. This atrophy is now widely accepted to be induced after activation of two well-known muscle-specific ubiquitin ligases, muscle RING finger-1 (MuRF-1) and muscle atrophy F-Box 1 (MAFbx, or Atrogin-1) [6]. Moreover, the two ligases are regulated by several regulators, including Forkhead box O3 (FoxO3a) [7, 8], and nuclear factor kappa B (NF-κB) [9, 10]. Existing studies have found that NF-κB and FoxO3a can promote the expression of Atrogin-1/ MuRF-1 and induce protein degradation and apoptosis, thus aggravating denervated muscular atrophy [7-10]. At the same time, inhibition of FoxO3a and NF-κB prevented atrophy [11].

In addition, stem cells of muscle, the satellite cells are activated under denervation and try to differentiate into myofibers to repair muscle loss. Unfortunately, this restorative phenomenon remains shortly and inadequately until timely, sufficient reinnervation, which is often unlikely after serious nerve injuries, responsible for the continuous atrophy of skeletal muscle [12].

HOXA9, a member of Hox genes, is a key regulator of stem cells and plays a positive role in regulating the development of muscles and limbs during embryogenesis, while it can only be detected in a few stem

cells after birth. Interestingly. HOXA9 is usually activated in several serious conditions such as cancer, leukemia, aging, and so on, showing a contrary effect: interference with the homeostasis of stem cells [13-15]. But its expressing and molecular basis in denervated muscles still remains unknown.

Here, we analyzed the express rules of HOXA9 and its promoters, MLL1and WDR5, in the rat gastrocnemius muscle after sciatic nerve operation, comparing denervation, reinnervation, and the general conditions. In addition, to furtherly investigate the effects of HOXA9 in skeletal muscles, experiments in vitro were performed in primary satellite cells.

Methods

Animal procedures

Male SD rats (200–250 g) were housed in a standard facility (23℃, 50% relative humidity, 12-h light/12-h dark cycle) and provided with adequate food and water. The rats were allocated randomly into the following groups (36 rats/group): denervation group; denervation + nerve repairing group (repairing); and sham operation group. Denervation and nerve repairing operations were performed surgically on the right hind legs as previously described [16][4]. Surgeries were conducted of mice under anesthetization with pentobarbital (50 mg/kg ip.). The sciatic nerve was separated and exposed via a lateral incision in the mid-thigh. Afterwards, in denervation group we removed 0.5 cm of the sciatic nerve and buried both ends in the muscles; in the repairing group, the nerve was cut in the middle, and the epineurium was then immediately sutured with 9-0 nylon thread; in the sham group, no neurotomy was carried out after exposed. After that, we closed the incision with a 4-0 absorbable suture. 6 rats of each group were euthanized at the indicated time post-operation (0d, 3d, 7d, 2w, 3w, 4w), and gastrocnemii on both sides were removed to assess atrophy.

Primary cell culture

Primary satellite cells were extracted from hind limb muscles of neonatal rats(<3d) as literature [17], and cultured at 37°C, 3% O_2, 5% CO_2, and 95% humidity. 0.1% type Ⅱcollagenase (Sigma) solution was used to digest tinily chopped muscles for 30 min. The mixture was then centrifuged (1000r/min,10 min) to remove the supernatant. Next, we added 0.25% trypsin (Sigma) solution to the precipitate. After 15 min of incubation, cells were centrifuged and separated again as above. We mixed 20% FBS (Gibco) with Dulbecco's Modified Eagle's Medium/Nutrient F-12 Ham (DMEM/F12ham, Solarbio, Beijing, China) to stop the digestion. Afterwards, the mixture was filtered by a 70-μm cell strainer, following a 40-μm cell strainer, and then centrifuged again (1000r/min, 10 min). The sediment was then suspended in the growth medium consisting of DMEM/F12ham, 20% FBS, and 1% penicillin/streptomycin (Solarbio). We transferred the suspended cells to a collagen-coated petri dish, where they were pre-attached for two hours to purify satellite cells [17]. After this, the supernatant containing the non-adherent cells was transferred to a new collagen-coated petri dish. The growth medium was changed every two days. The cells were used in subsequent experiments upon reaching approximately 60%–70% confluence. To verify

the purity of satellite cells, immunofluorescence staining with Desmin protein, a myogenic marker which expressed early in early stages of satellite cells' differentiation [18], was performed.

Immunofluorescence (IF)

Primary satellite cells were fixed in 4% paraformaldehyde (Boster Biological Technology, Wuhan, China) at room temperature for 15 min. After washed with PBS (Boster), the adherent cells were permeabilized (0.1% Triton X-100 in PBS, Boster), blocked (10% normal goat serum in PBS, Solarbio), and incubated at 4 C overnight with primary antibody (Desmin; 1:50; ab32362; Abcam). After washing with PBS, secondary antibody Goat Anti-Rat IgG H&L (Alexa Fluor 488) (1:200, ab150157, Abcam) was applied. Following three washes with PBS, cells were treated with antifade Mounting Medium containing DAPI (Beyotime). The section was scanned on a digital slice scanning system Pannoramic MIDI (3DHISTECH Ltd, Hungary) and image analysis was performed using its analysis software Caseviewer 2.2 (3DHISTECH Ltd, Hungary).

Plasmids and transfection

shRNA of HOXA9 (target: AAGTGTGAGTGTCAAGCGT) was inserted into the pPLK/GFP-Puro plasmids, and the coding region sequence of rat HOXA9 was cloned into the pires2-dsred2 vector to produce a recombinant HOXA9 construct (Public Protein/Plasmids Library, China). Primary satellite cells were divided into 4 groups: transfected respectively with pIRES2-DsRed2 empty plasmids, pIRES2-DsRed2-HOXA9 plasmids, pPLK/GFP-Puro empty plasmids, and pPLK/GFP-Puro- HOXA9 shRNA plasmids. The transfection was carried out through Lipofectamine 3000 (Invitrogen, Carlsbad, CA, USA) according to the standard manufacturer's protocols. The TUNEL staining, western blot, and rt-PCR were executed 36 h after transfection. Photographs were taken with a Leica DM6B microscope (Leica, Wetzlar, Germany).

Wet weight ratio

The gastrocnemius muscles of the surgical side and contralateral side were both taken, washed with normal saline, dried with filter paper, and weighed. The wet weight ratio was calculated by dividing the muscle weight of the operative side by that of the contralateral side.

Immunohistochemistry of paraffin sections

Mid-portions of the operational gastrocnemii were fixed through paraformaldehyde (4%), then dehydrated, and paraffin-embedded. 5-μm thick cross-sectional slices of the muscle wax samples were made on a slicing machine (Leica Biosystems, Germany). Following deparaffinage, hydration, heat mediated antigen retrieval (Tris/EDTA buffer PH 9.0, Solarbio), endogenous peroxidase activity blocking, and goat serum blocking, primary rabbit anti-HOXA9 (1:500; NBP2-32356, Novus, US) incubation was conducted overnight at 4 °C. After application of HRP-labeled Goat Anti-Rabbit IgG(H+L) (1:50, Beyotime, Haimen, China), diaminobenzidine working solution (DAB Horseradish Peroxidase Color Development Kit, Beyotime), the sections were counter-stained with hematoxylin. Images were scanned and analyzed through Pannoramic MIDI (3DHISTECH Ltd, Hungary) and Caseviewer 2.2 (3DHISTECH Ltd, Hungary).

Quantification of fiber diameter

Hematoxylin staining in HOXA9 immunohistochemical staining makes each part of the sections clearly visible. Based on this, Muscle fiber diameters were calculated and analyzed. The diameter was determined in Caseviewer 2.2 (3DHISTECH Ltd, Hungary), and the average diameter of every fiber was expressed as a mean of three measurements. At least 600 total muscle fibers from six fields of each section were assessed.

Western blot

Western blot analysis was performed as previously described [4]. Proteins were harvested from primary satellite cells or gastrocnemius muscles with Whole Cell Lysis Assay (KGP2100, KeyGEN BioTECH, China). An equal amount of total protein was added per lane to subject into SDS-PAGE and then transferred onto PVDF membranes (Millipore Corp, US), which were followed by blocking with 5% nonfat dry milk dissolve in Tris-buffer saline (TBS). Afterwards, membranes were incubated at 4◦C overnight with primary antibodies: rabbit anti-HOXA9 (1:1000; NBP2-32356; Novus, US), rabbit anti-MLL1(1:1000; 14197S; Cell Signaling Technology, USA), rabbit anti- WDR5(1:1000; ab22512; Abcam, UK), rabbit anti-GAPDH(1:10000; ab181602; Abcam, UK), mouse anti-Myod(1:1000; ab16148; Abcam, UK), mouse anti-Myogenin(1:250; ab1835; Abcam, UK), rabbit anti- Wnt3a(1:1000; ab219412; Abcam, UK), rabbit anti-β-catenin(1:5000; ab32572; Abcam, UK), rabbit anti-P-β-catenin(1:500; ab75777; Abcam, UK), rabbit anti-Pax7(1:1000; ab92317; Abcam, UK), rabbit anti-Atrogin-1(1:1000; AP2041; ECM Biosciences, US), rabbit anti-MuRF-1(1:1000; MP3401; ECM Biosciences, US), rabbit anti-FoxO3a(1:1000; ab17026; Abcam, UK), rabbit anti-P-FoxO3a(1:500; ab47285; Abcam, UK), rabbit anti-NF-κB(1:500; ab16502; Abcam, UK), rabbit anti-P-NF-κB(1:1000; ab86299; Abcam, UK). After 3 washes, blots were incubated at 37◦C for 2h with appropriate secondary antibodies: HRP-labeled Goat Anti- Mouse IgG (H+L) (1:5000; Beyotime), or HRP-labeled Goat Anti-Rabbit IgG(H+L) (1:2000; Beyotime). Immunoreactive bands were developed by an enhanced chemiluminescence (ECL) kit (AR1171; Boster, China) and visualized through Chemidoc™ XRS+ (BIORAD, USA). The gray value of bands was analyzed with Image Lab 6.0.0 (BIORAD, USA).

RT-PCR

Total RNA from gastrocnemius muscles was extracted using the RNA Extraction Kit (Code No. 9767; Takara, Japan). cDNA was synthesized using the primescript™ RT Master Mix (Code No. RR036A; Takara, Japan), and RT-PCR was performed through SYBR® Premix Ex Taq™ II (Code No. RR820A; Takara, Japan) with the Applied Biosystems™ quantstudio™ 6 Flex Real-Time PCR System (Thermo Fisher Scientific, Germany). The primers were as follows: HOXA9, forward 5'-GAGAATGAGAGCGGTGGAGACAAG-3'and reverse 5'-CGAGTGGAGCGAGCATGTAGC-3'; MLL1, forward 5’-CCATGAGGACAAGAAGCGGAAGG-3’ and reverse 5’-GCACTAGCGGCAAGAGGACTAAC-3’; WDR5, forward 5'-GCCAACTTCTCCGTGACAGGTG-3' and reverse 5'-TCTAACGCTGCTGAGGCAATGATG-3'; GAPDH, forward 5’-ATGACTCTACCCACGGCAAG-3’ and reverse 5’-GGAAGATGGTGATGGGTTTC-3’. Relative gene expression levels of mRNA were calculated using the ΔΔCt-method, with GAPDH as an internal control for normalization.

TUNEL staining TUNEL assay

In satellite cells 36h after transfection, the TUNEL assay was performed using the In Situ Cell Apoptosis Detection Kit I (POD) (Boster, China) as the specification requested.

Statistical analysis

Statistical analysis was carried out using the Graphpad Prism 7 Software (US) with all data shown as mean ± standard deviation calculated from at least six independent experiments. Each experimental measure was performed in triplicate. Results were analyzed using the One-way ANOVA when coming from three or more groups and using the t-test when from two experimental groups. $P < 0.05$ was considered statistically significant.

Results

Analysis of muscular atrophy after sciatic nerve operations

Wet weight and fiber diameter

Wet weight analysis (figure 1.A) revealed muscle atrophy in denervated and repaired muscles from 3d to 8w by the wet weight ratio (operational weight divided by specific weight). Consistent with previous research [4], gastrocnemius at the side of denervation operation atrophied rapidly; while in the repairing group, the mass loss was rescued after 2 weeks post-operation but still more serious than the sham group. The result showed the denervated atrophy was a gradual slowdown, with muscle wet weight dropping rapidly in the first 2 weeks (gastrocnemius muscle decreased by an average of 57%), then gradually in the second 2 weeks (average 17%) and only 11% over the following 4 weeks.

To confirming the above results furtherly, fiber diameter analysis (figure 1.B) was performed according to the immunohistochemical results of HOXA9 (figure 2.A). Fiber diameter increased obviously over time in the sham group, but it was reduced contrastly in both denervation and repairing groups. Furthermore, the histograms of the denervation group shifted to the left as a consequence of a larger proportion of small fibers; while in the repairing group, it was revived after 2 weeks, and the diameter distribution was more and more similar to the sham group as time goes.
Regulation of the HOXA9 system

Immunohistochemical staining (figure 2.A) showed that the HOXA9 protein expression increased substantially post-denervation; while it was biphasic post-repairing, with a less obvious increment in the first 3 weeks and then a gradual reduction over the following time; but it’s not adjusted clearly post-sham operation. Moreover, the immunohistochemical staining revealed more and more HOXA9 distribution in the nucleus and cytoplasm with the process of atrophy induced by denervation, while only few expression was detected in the nucleus in the other two groups.

Western blots (figure 2.B, C) of HOXA9 and its promoting factors, MLL1 and WDR5, were performed at the indicated time. HOXA9 protein expressed as immunohistochemical showed. MLL1 protein showed a tendency of increasing first and then decreasing later after denervation, reaching the peak at 4w post-denervation; in repairing group, MLL1 showed a little increment at 3d post-repairing but No significant change at other points. WDR5 seemed much less responsive to denervation or repairing, and statistically significant changes were only detected at 4w, 8w post-denervation (1.71, 2.44 times that of 0d) and 1w post-repairing (1.17 times that of 0d).

A time-course mRNA expression analysis of HOXA9, MLL1, WDR5 was also assessed (figure 2.D). HOXA9, MLL1, WDR5 mRNA expression was similar in denervation and repairing groups, upregulated after the operation and reaching the peak at a special point: MLL1 at 2w, WDR5 at 4w post-denervation; HOXA9, MLL1, WDR5 at 2w post-repairing. Especially, until 8w post-operation, the peak of HOXA9 mRNA still has not been seen in the denervation group. Moreover, at 8w post-repairing all of HOXA9, MLL1, WDR5 mRNA returned to an expression level comparable to the sham group, but still a high level in the denervation group.

In vitro analysis of HOXA9 effects on satellite cells

To deeply study the HOXA9 system in muscle, we performed experiments in vitro using primary satellite cells from the hind limbs of newborn rats. Immunofluorescence staining showed a good purity of muscle satellite cells (figure 3.A). In this model, overexpression and knockdown of HOXA9 were mediated through plasmids and detected 36h after transfected, showing a satisfactory overexpression average 4.16-fold at protein levels and 2750.83-fold at mRNA levels, and knockdown to 42.69% at protein levels and 48.75% at mRNA levels (figure 3.B-E).

HOXA9 inhibits myogenic differentiation but not damage the differentiation potential of satellite cells

Indicators of myogenic differentiation, Myod and Myogenin [19, 20], showed inhibited averagely to 38.29% (Myod) and 79.97% (Myogenin) by pIRES2-DsRed2-HOXA9 plasmids, while pPLK/GFP-Puro-HOXA9 shRNA plasmids could rescue them to 116.10% (Myod) and 137.24% (Myogenin) (figure 4. A-C).

Furthermore, the inhibiting signal pathway of myogenic differentiation, Wnt-[21, 22], was also detected. Unsurprisingly, Wnt3a and β-catenin had an increased expression after pIRES2-DsRed2-HOXA9 plasmids transfection (Wnt3a to 130.12% and β-catenin to 143.33 %), and a decreased expression after pPLK/GFP-Puro- HOXA9 shRNA plasmids transfection (Wnt3a to 68.28% and β-catenin to 80.40 %). Though the P- β-catenin didn't increase typically after pires2-dsred2-HOXA9, it showed a statistically significant reduction to 67.86 % after pPLK/GFP-Puro- HOXA9 shRNA (figure 4. D-G).

Interestingly, Pax7, which reflects the differentiation potential of satellite cells [23], didn't change statistically by either pIRES2-DsRed2-HOXA9 or pPLK/GFP-Puro- HOXA9 shRNA plasmids (figure 4. H+I).

These data suggested that HOXA9 inhibited myogenic differentiation in satellite cells, but it didn't damage the differentiation capacity.

HOXA9 promotes atrophy in satellite cells

Two muscle-specific E3 ubiquitin ligases Atrogin-1 and MuRF-1 were both upregulated by pIRES2-DsRed2-HOXA9 (Atrogin-1 to 161.64% and MuRF-1 to 192.66 %), and MuRF-1 was inhibited to 47.90 % by pPLK/GFP-Puro- HOXA9 shRNA. No significant difference of Atrogin-1 was found between pPLK/GFP-Puro- HOXA9 shRNA and pPLK/GFP-Puro (figure 5. A-C).

P-FoxO3a (figure 5.D+E) and p-NF-κB (figure 5.F+G) relative expressions showed similar changes after transfection: increased significantly after pIRES2-DsRed2-HOXA9 (P-FoxO3a to 474.77% and p-NF-κB to 175.07 %), and decreased after pPLK/GFP-Puro- HOXA9 shRNA (P-FoxO3a to 18.07% and p-NF-κB to 78.99 %).

Thus, it can be seen that HOXA9 could influence the typical atrophy pathways and lead to atrophy in satellite cells.

HOXA9 promotes apoptosis of satellite cells

Additionally, we analyzed the percentage of apoptotic cells by TUNEL staining. Differences between pires2-dsred2-HOXA9 and pires2-dsred2 (figure 6. A+B), between pPLK/GFP-Puro- HOXA9 shRNA and pPLK/GFP-Puro (figure 6. C+D) were found, showing that HOXA9 induced apoptosis in satellite cells.

Discussion

The purpose of this study was to investigate the mechanism of HOXA9 in skeletal muscles after peripheral nerve injury and reinnervation. To explore the molecular changes occurring in denervated and reinnervated muscles, we made use of three models of median nerve surgeries models to simulate the most common clinical conditions, namely denervation (peripheral nerve injury), repairing (peripheral nerve injury followed by surgical reconstructive surgery) and sham (the general population).

We analyzed the muscle wet weight ratio and fiber diameter to follow histological changes in these three conditions. In this study, we found that the muscle atrophy worsened over time after denervation, while the shrinking trend was restored from 3w post repairing. The muscle fiber size distribution confirmed these data: at 3w, 4w, 8w post-operation, the distribution was gradually similar between the repairing and the sham groups; in contrast, in denervated muscles, the number of smaller fibers was higher, consistent with literature data [24].

Denervation has been reported to increase the sensitivity of satellite cells to apoptosis [25, 26], which may result in the inability of muscle regeneration after a long period of time without nerve input. And the activation of satellite cells is a significant pathway of muscle recovery after denervated [27]. HOXA9 belonging to the HOX gene family is a key regulator of stem cells and tissue patterning during embryogenesis, playing roles either as an oncogene or as a tumor suppressor in various tumors [28]. Its involvement in cancers is well studied [29-31]. Since Simon Schwoerer's discovery that HOXA9 was particularly activated in aged skeletal muscle and limited satellite cells' function and muscle regeneration

by activating senescence-related signaling pathways [15], the mechanism of HOXA9 in skeletal muscle has attracted extensive attention, but it is still little known after nerve injury.

We have demonstrated for the first time that HOXA9 is regulated in denervated and reinnervated skeletal muscle. We found the HOXA9 protein, not its upstream regulator MLL1 or WDR5, kept pace with the extent of muscle atrophy in a sense, continuing to increase after denervation, reaching a peak at 3w post repairing and then decreasing gradually to baseline, changed insignificantly in the sham group. Moreover, HOXA9 protein expressions seemed to be less after repairing than the denervation group in the case of a similar degree of muscular atrophy (3d, 1w, 2w), though the statistical difference was only detected at 2w. In particular, HOXA9 protein in the repairing group decreased to the control group level at 8w post-operation, while the wet weight ratio still lower than the sham muscle, showing asynchronous to atrophy and relative irreversibility of muscle injury after serious nerve injury in the long-term analysis. These data suggested there must be some mechanism between HOXA9 protein and denervated muscle atrophy. Considering the regulatory effect of HOXA9 on stem cells, is it through the regulation of satellite cells? The vitro experiments confirmed this assumption. HOXA9 inhibited myogenic differentiation, affected the classical signaling pathway of muscular atrophy, and induced apoptosis of satellite cells, but the Pax7 showed no significant change, meant the differentiation potential of the remaining satellite cells had not weakened nor disappeared. In summary, HOXA9 seemed to inhibit the development process of satellite cells towards myotubes without damaging its activity of differentiation. Coincidentally, satellite cells from denervated muscles were able to differentiate in culture even after up to seven months of denervation [32], but it is unattainable in vivo [33]. There must be special mechanisms in vivo which regulate satellite cell activity after peripheral nerve injury and determines the fate of the muscle. Is it HOXA9? Maybe, but this will require further verifications.

There are still some questions here. First of all, the spatial distribution of HOXA9 protein after denervation, especially at 4w and 8w, a large part of which was located in the cytoplasm rather than the nuclear, was significantly different from the other groups in which HOXA9 protein was mainly located in the nucleus. At the same time, HOXA9 protein in the nuclear also increases with the aggravation of muscular atrophy in both denervation and repairing groups. It may be that HOXA9 in the cytoplasm is an activated form or some metabolites. However, no further research was carried out in this study. Besides, in vitro experiments, HOXA9 mRNA expression level in the pIRES2-DsRed2-HOXA9 group increased abnormally to as much as 2750.83 times, while the HOXA9 protein increased to only 4.16 times. We suspect that there are mechanisms in cells that we have not found that inhibit HOXA9 activity and maintain the stability of the intracellular environment. This may be related to the silence of HOXA9 after birth in vivo. But we have no evidence for that at the moment.

Conclusion

To summarize, this study revealed the modulation of HOXA9 after skeletal muscle denervation/reinnervation and explored the inhibition of HOXA9 on myogenic repair function of satellite

cells, showing a new system centered on HOXA9 which targets satellite cells and provides a new clinical idea for the treatment of denervated muscle.

Abbreviations

Hoxa9: Homeobox A9; MLL1: Mixed Lineage Leukemia 1; WDR5: WD-40 repeat protein 5; DsRed2: red fluorescent protein 2; GFP: green fluorescent protein; shRNA: short hairpin RNA; MuRF-1: muscle RING finger-1; MAFbx or Atrogin-1: muscle atrophy F-Box 1; FoxO3a: Forkhead box O3; NF-Kb: nuclear factor kappa B; FBS: fetal bovine serum; DMEM/F12ham: Dulbecco's Modified Eagle's Medium/Nutrient F-12 Ham; PBS: phosphate buffer saline; IgG: immunoglobulin G; IF: immunofluorescence; TUNEL: TdT (Terminal Deoxynucleotidyl Transferase)-mediated dUTP Nick-End Labeling; rt-PCR: reverse transcription Polymerase Chain Reaction (PCR) ; EDTA: ethylenediaminetetraacetic acid; DAB: 3,3'-diaminobenzidine; SDS-PAGE: SDS-polyacrylamide gel electrophoresis; PVDF: vinylidene fluoride; TBS: Tris-buffer saline; HRP: Horseradish Peroxidase; ECL: enhanced chemiluminescence; cDNA: complementary DNA; ANOVA: Analysis of Variance; Myod: myostatin and myoblast differentiation factor; Pax7: paired-box transcription factor 7

Declarations

Ethics approval and consent to participate

This study was approved by the Animal Use Committee at Shanxi medical university (code: 2016LL083, March 14, 2016) and was performed in compliance with the World Health Organization (WHO) International Guiding Principles for Animal Research.

Consent for publication

Not applicable.

Availability of data and materials

The datasets during and/or analyzed during the current study available from the corresponding author on reasonable request.

Competing interests

The authors declare that they have no competing interests

Funding

This study was funded by the Opening Project (17DZ2270500) from the Key Laboratory of Hand Reconstruction, Ministry of Health, and Shanghai Key Laboratory of Peripheral Nerve and Microsurgery,

Shanghai, People's Republic of China; funded by the National Natural Science Foundation of China (81171722). The authors declare that there is no conflict of interest.

Authors' contributions

XML and WKC designed the study. XML and SJL performed the experiments. BSL and ZC helped with data analysis. XML wrote the manuscript. All authors read and approved the final manuscript.

Acknowledgements

Not applicable.

References

1. KD, B., A. M, M. S, V. I, M.-S. K, U. E, B. RA, S. C, R. O, S. S, et al., *Peripheral nerve transfers change target muscle structure and function.* Science advances, 2019. **5**(1): p. eaau2956.
2. Y, S., Z. R, X. L, W. Q, Z. J, G. J, H. Z, M. W, S. M, D. F, et al., *Microarray Analysis of Gene Expression Provides New Insights Into Denervation-Induced Skeletal Muscle Atrophy.* Frontiers in physiology, 2019. **10**: p. 1298.
3. S, C., N. JA and G. AL, *Muscle wasting in disease: molecular mechanisms and promising therapies.* Nature reviews. Drug discovery, 2015. **14**(1): p. 58-74.
4. Yang, X., P. Xue, X. Liu, X. Xu and Z. Chen, *HMGB1/autophagy pathway mediates the atrophic effect of TGF-beta1 in denervated skeletal muscle.* Cell Commun Signal, 2018. **16**(1): p. 97.
5. Morano, M., G. Ronchi, V. Nicolo, B.E. Fornasari, A. Crosio, I. Perroteau, S. Geuna, G. Gambarotta and S. Raimondo, *Modulation of the Neuregulin 1/ErbB system after skeletal muscle denervation and reinnervation.* Sci Rep, 2018. **8**(1): p. 5047.
6. SC, B., L. E, B. S, L. VK, N. L, C. BA, P. WT, P. FJ, N. E, D. K, et al., *Identification of ubiquitin ligases required for skeletal muscle atrophy.* Science (New York, N.Y.), 2001. **294**(5547): p. 1704-8.
7. M, S., S. C, G. A, S. C, C. E, P. A, W. K, S. S, L. SH and G. AL, *Foxo transcription factors induce the atrophy-related ubiquitin ligase atrogin-1 and cause skeletal muscle atrophy.* Cell, 2004. **117**(3): p. 399-412.
8. J, Z., B. JJ, S. A and G. AL, *Coordinate activation of autophagy and the proteasome pathway by FoxO transcription factor.* Autophagy, 2008. **4**(3): p. 378-80.
9. F, M., K. P, L. T, S. YH, D. P, A. R, P. V, B. R, P. M and R. N, *Targeted ablation of IKK2 improves skeletal muscle strength, maintains mass, and promotes regeneration.* The Journal of clinical investigation, 2006. **116**(11): p. 2945-54.
10. D, C., F. JD, T. NE, M. PA, O. BC, L. HG, H. PO, F. WR, L. J, G. DJ, et al., *IKKbeta/NF-kappaB activation causes severe muscle wasting in mice.* Cell, 2004. **119**(2): p. 285-98.
11. SM, S., D. SL, M. JM and J. AR, *Hsp70 overexpression inhibits NF-kappaB and Foxo3a transcriptional activities and prevents skeletal muscle atrophy.* FASEB journal : official publication of the Federation

of American Societies for Experimental Biology, 2008. **22**(11): p. 3836-45.

12. Kostrominova, T.Y., *The Biology and Restorative Capacity of Long-Term Denervated Skeletal Muscle.* 2002. **12**: p. 247-254.
13. An, T.W., B.A. Evanoff, M.I. Boyer and D.A. Osei, *The Prevalence of Cubital Tunnel Syndrome: A Cross-Sectional Study in a U.S. Metropolitan Cohort.* J Bone Joint Surg Am, 2017. **99**(5): p. 408-416.
14. Foad, S.L., C.T. Mehlman and J. Ying, *The epidemiology of neonatal brachial plexus palsy in the United States.* J Bone Joint Surg Am, 2008. **90**(6): p. 1258-64.
15. Schworer, S., F. Becker, C. Feller, A.H. Baig, U. Kober, H. Henze, J.M. Kraus, B. Xin, A. Lechel, D.B. Lipka, et al., *Epigenetic stress responses induce muscle stem-cell ageing by Hoxa9 developmental signals.* Nature, 2016. **540**(7633): p. 428-432.
16. Saito, H. and L.B. Dahlin, *Expression of ATF3 and axonal outgrowth are impaired after delayed nerve repair.* BMC Neurosci, 2008. **9**: p. 88.
17. Dai, J.M., M.X. Yu, Z.Y. Shen, C.Y. Guo, S.Q. Zhuang and X.S. Qiu, *Leucine Promotes Proliferation and Differentiation of Primary Preterm Rat Satellite Cells in Part through mTORC1 Signaling Pathway.* Nutrients, 2015. **7**(5): p. 3387-400.
18. Liu, Y., S. Chen, W. Li, H. Du and W. Zhu, *Isolation and characterization of primary skeletal muscle satellite cells from rats.* Toxicol Mech Methods, 2012. **22**(9): p. 721-5.
19. Tosic, M., A. Allen, D. Willmann, C. Lepper, J. Kim, D. Duteil and R. Schule, *Lsd1 regulates skeletal muscle regeneration and directs the fate of satellite cells.* Nat Commun, 2018. **9**(1): p. 366.
20. Schaaf, G.J., T.J. van Gestel, E. Brusse, R.M. Verdijk, I.F. de Coo, P.A. van Doorn, A.T. van der Ploeg and W.W. Pijnappel, *Lack of robust satellite cell activation and muscle regeneration during the progression of Pompe disease.* Acta Neuropathol Commun, 2015. **3**: p. 65.
21. Cui, S., L. Li, S.N. Mubarokah and R. Meech, *Wnt/beta-catenin signaling induces the myomiRs miR-133b and miR-206 to suppress Pax7 and induce the myogenic differentiation program.* J Cell Biochem, 2019. **120**(8): p. 12740-12751.
22. AS, B., C. MJ, R. S, L. M, K. CJ, K. C and R. TA, *Increased Wnt signaling during aging alters muscle stem cell fate and increases fibrosis.* Science (New York, N.Y.), 2007. **317**(5839): p. 807-10.
23. Rao, L., Y. Qian, A. Khodabukus, T. Ribar and N. Bursac, *Engineering human pluripotent stem cells into a functional skeletal muscle tissue.* Nat Commun, 2018. **9**(1): p. 126.
24. G, L., Z. M, L. JY, O. S, X. H, L. N, Y. Y, L. X and Z. L, *Proteomics and Transcriptomics Analysis Reveals Clues into the Mechanism of the Beneficial Effect of Electrical Stimulation on Rat Denervated Gastrocnemius Muscle.* Cellular physiology and biochemistry : international journal of experimental cellular physiology, biochemistry, and pharmacology, 2019. **52**(4): p. 769-786.
25. SS, J., M. CL and K. WM, *Skeletal muscle denervation increases satellite cell susceptibility to apoptosis.* Plastic and reconstructive surgery, 2002. **110**(1): p. 160-8.
26. SS, J. and K. WM, *Satellite cell depletion in degenerative skeletal muscle.* Apoptosis : an international journal on programmed cell death, 2003. **8**(6): p. 573-8.

27. Agüera, E., S. Castilla, E. Luque, I. Jimena, I. Ruz-Caracuel, F. Leiva-Cepas and J. Peña, *Denervated muscle extract promotes recovery of muscle atrophy through activation of satellite cells. An experimental study.* Journal of sport and health science, 2019. **8**(1): p. 23-31.
28. Fu, Z., C. Chen, Q. Zhou, Y. Wang, Y. Zhao, X. Zhao, W. Li, S. Zheng, H. Ye, L. Wang, et al., *LncRNA HOTTIP modulates cancer stem cell properties in human pancreatic cancer by regulating HOXA9.* Cancer Lett, 2017. **410**: p. 68-81.
29. Collins, C.T. and J.L. Hess, *Role of HOXA9 in leukemia: dysregulation, cofactors and essential targets.* Oncogene, 2016. **35**(9): p. 1090-8.
30. Rusan, M., R.F. Andersen, A. Jakobsen and K.D. Steffensen, *Circulating HOXA9-methylated tumour DNA: A novel biomarker of response to poly (ADP-ribose) polymerase inhibition in BRCA-mutated epithelial ovarian cancer.* Eur J Cancer, 2019. **125**: p. 121-129.
31. Han, S., X. Li, X. Liang and L. Zhou, *HOXA9 Transcriptionally Promotes Apoptosis and Represses Autophagy by Targeting NF-kappaB in Cutaneous Squamous Cell Carcinoma.* Cells, 2019. **8**(11).
32. AB, B., D. El and C. BM, *Differentiation of activated satellite cells in denervated muscle following single fusions in situ and in cell culture.* Histochemistry and cell biology, 2005. **124**(1): p. 13-23.
33. AB, B., D. El and C. BM, *Abortive myogenesis in denervated skeletal muscle: differentiative properties of satellite cells, their migration, and block of terminal differentiation.* Anatomy and embryology, 2005. **209**(4): p. 269-79.

Figures

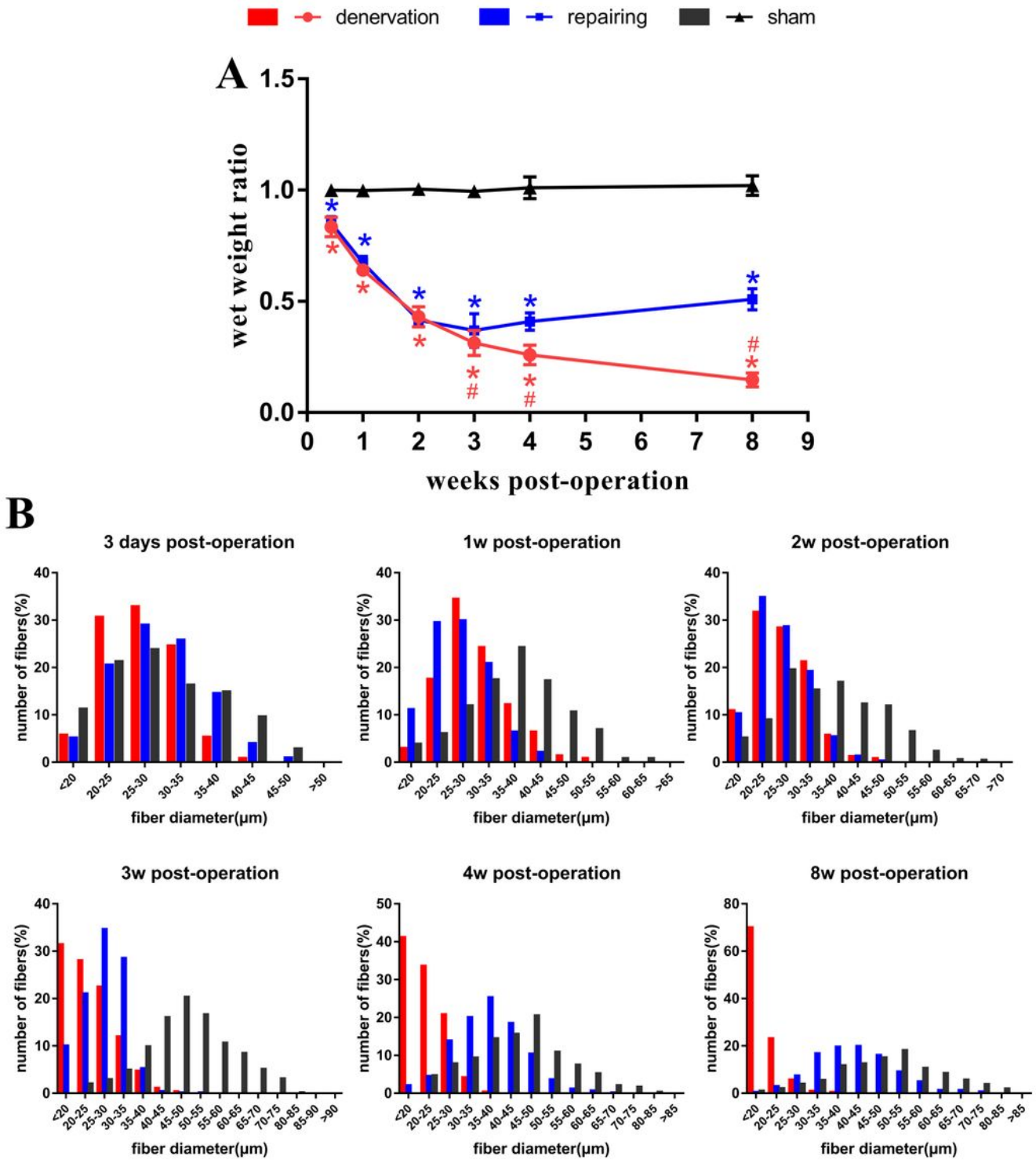

Figure 1

Wet weight and fiber diameter analysis of denervated and reinnervated muscles. A Wet weight ratio (weight on the surgical side divided by weight on the contralateral side) of gastrocnemius at indicated time. 6 rats/group. *P < 0.05 vs sham group. #P < 0.05 denervation vs repairing group. B Quantification of muscle fibers diameter from Immunohistochemical staining of HOXA9(figure 2. A). Denervation 3d

n=940, 1w n=952, 2w n=843, 3w n=828, 4w n=843 ,8w n=749; repairing 3d n=852, 1w n=762, 2w n=1071, 3w n=800, 4w n=780 ,8w n=650; sham 3d n=987, 1w n=854, 2w n=680, 3w n=650, 4w n=962 ,8w n=745.

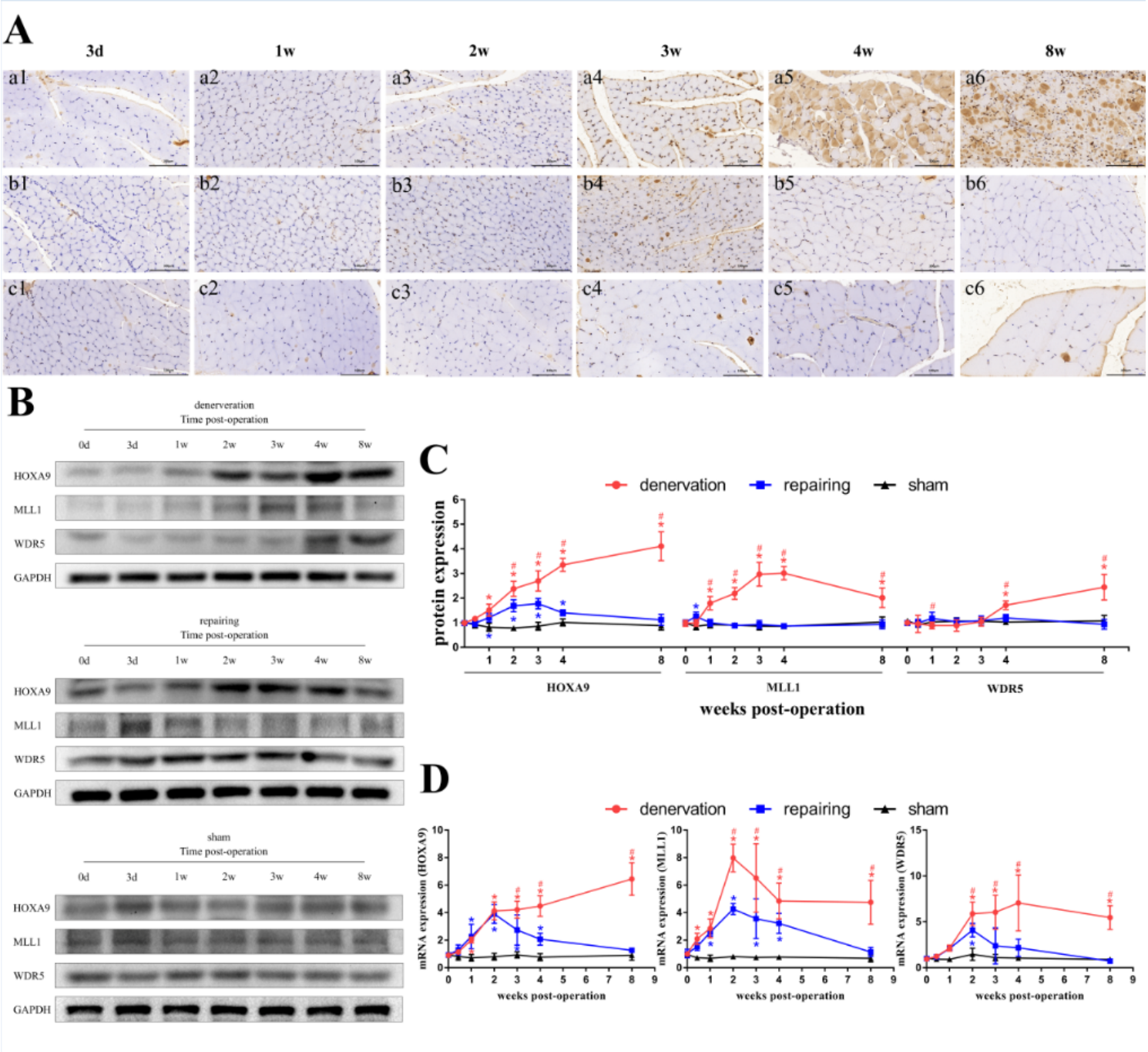

Figure 2

Expression analysis of Hoxa9 and its promoting factors, MLL1 and WDR5, after denervation and reinnervation. A Immunohistochemistry staining of HOXA9 in gastrocnemius post-operation (denervation: a1-a6; repairing: b1-b6; sham:c1-c6). Scale bar:100μm. B+C Western blot and relative grey value analysis of HOXA9, MLL1, and WDR5 protein relative expression in gastrocnemius post-operation. GAPDH was used as the loading control. D real-time PCR analysis of HOXA9, MLL1, and WDR5 mRNA relative expression in gastrocnemius at different time post-operation. GAPDH was used as the loading control. 6 rats/group. *P < 0.05 vs sham group. #P < 0.05 denervation vs repairing group.

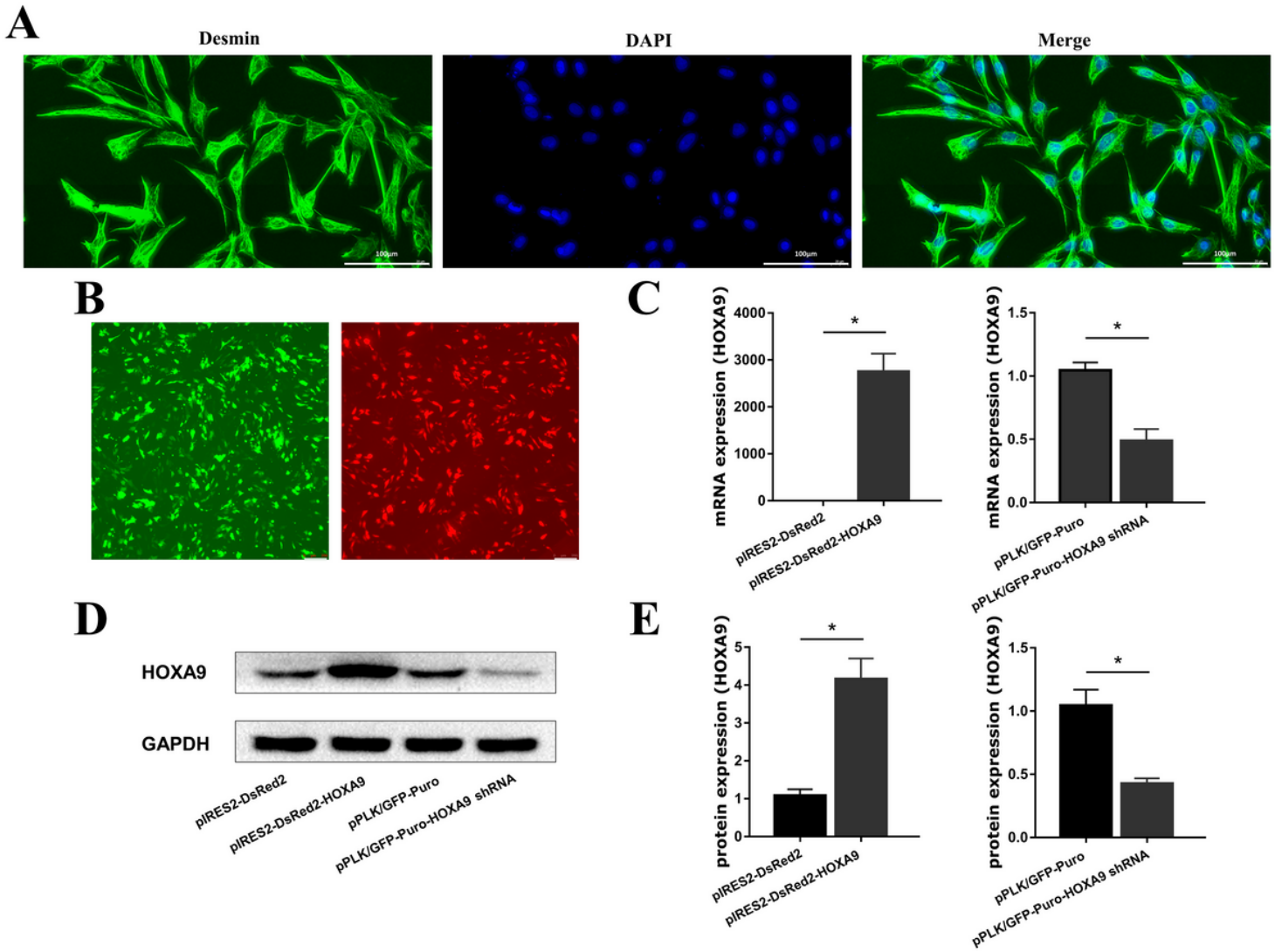

Figure 3

A Desmin immunostaining of primary satellite cells. Scale bar: 100 μm. B Primary satellite cells were transfected with the plasmids described above for 36 hours and imaged on a confocal microscope. Representative confocal microscopy images of GFP (green) and DsRed2 (red) are shown. Scale bar: 250 μm. C Relative expression levels of Hoxa9 mRNA after transfection by real-time PCR in four groups. D+E Protein expression levels of Hoxa9 were assessed after transfection by western blot. GAPDH was used as the loading control. N=6. *P < 0.05.

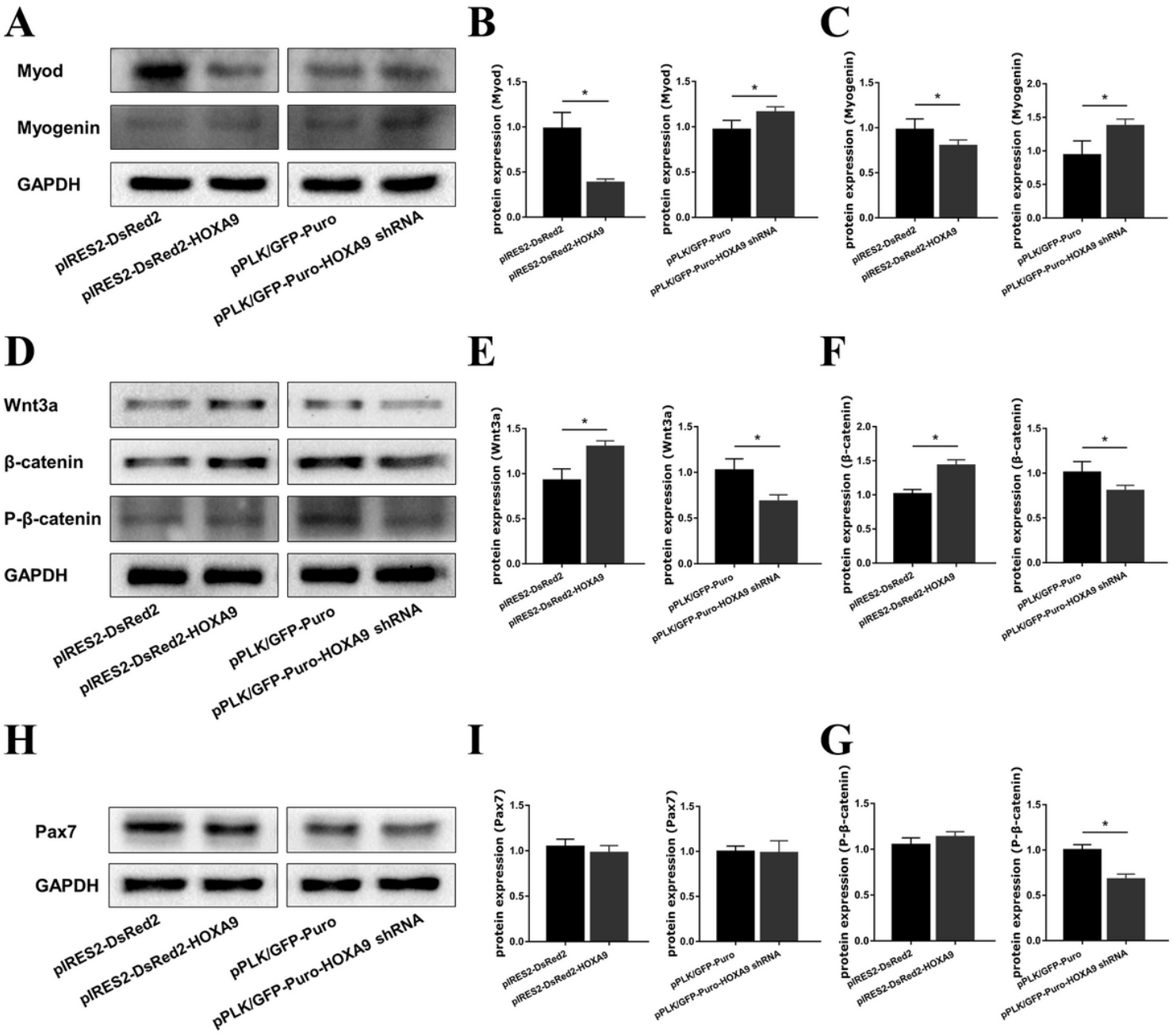

Figure 4

Hoxa9 inhibits myogenic differentiation of satellite cells. Relative expression of Myod and Myogenin(A-C), Wnt-(D-G), and Pax7(H+I) measured by western blot analysis after transfection. GAPDH was used as a loading control. N=6. *P < 0.05.

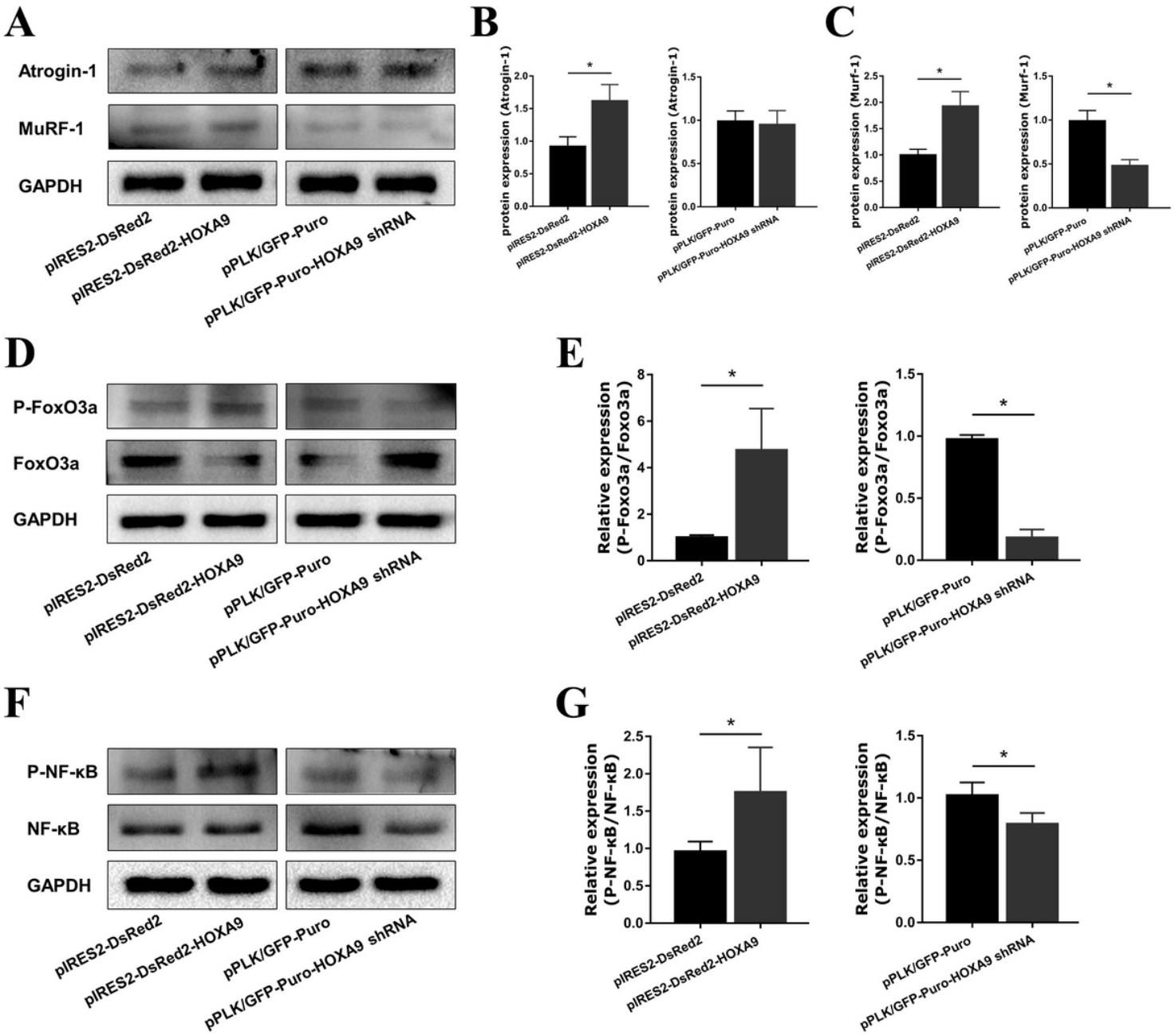

Figure 5

Hoxa9 can promote skeletal muscle atrophy. Relative expression of Atrogin-1 and MuRF-1(A-C), FoxO3a and P-FoxO3a(D+E), NF-κB, and P-NF-κB(F+G), in primary satellite cells after transfection measured by western blot analysis. GAPDH was used as a loading control. N=6. *P < 0.05.

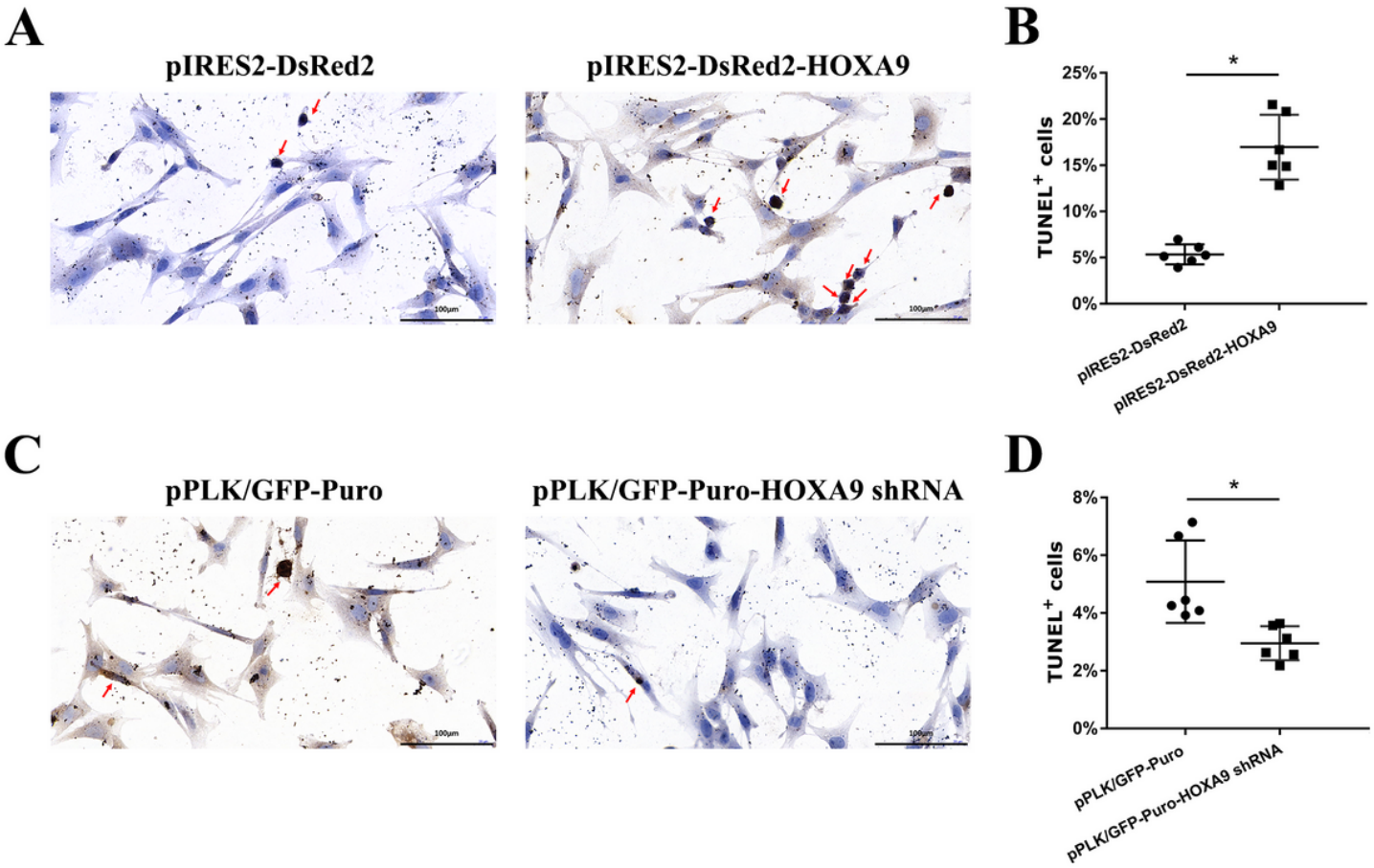

Figure 6

HOXA9 promotes satellite cell apoptosis. A+C TUNEL staining of satellite cells overexpressed or inhibited Hoxa9. Red arrowheads indicated TUNEL positive cells. Scale bar: 100 μm. B+D Quantification of apoptosis based on TUNEL staining as in A or C. A total of 6 fields per group were analyzed. *P < 0.05.